NASA CONTRACTOR
REPORT

NASA CR-129038

(NASA-CR-129038) RESEARCH STUDY ON MATERIALS PROCESSING IN SPACE EXPERIMENT NUMBER M512: NICKEL - 12 wt PERCENT TIN ALLOY EVALUATION Summary (Grumman Aerospace Corp.) 19 p HC $3.25 CSCL 22B

N75-10119

G3/12

Unclas
52680

RESEARCH STUDY ON MATERIALS PROCESSING IN SPACE EXPERIMENT NUMBER M512

Nickel - 12 Wt. Percent Tin Alloy Evaluation

By David J. Larson, Jr., and Chou H. Li
Grumman Aerospace Corporation
Bethpage, N.Y. 11714

December 1973

Summary Report

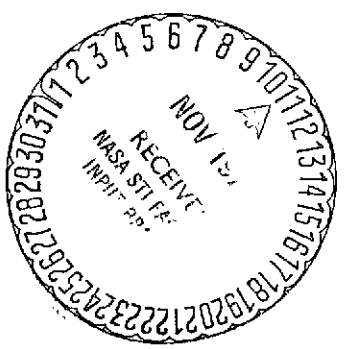

Prepared for

NASA-GEORGE C. MARSHALL SPACE FLIGHT CENTER
Marshall Space Flight Center, Alabama 35812

TECHNICAL REPORT STANDARD TITLE PAGE

1. REPORT NO.	2. GOVERNMENT ACCESSION NO.	3. RECIPIENT'S CATALOG NO.
NASA CR-129038		

4. TITLE AND SUBTITLE
Title: Research Study on Materials Processing in Space
Experiment Number M512
Subtitle: Nickel - 12 Wt% Tin Alloy Evaluation

5. REPORT DATE: December 1973

6. PERFORMING ORGANIZATION CODE

7. AUTHOR(S): David J. Larson, Jr.; Chou H. Li

8. PERFORMING ORGANIZATION REPORT #

9. PERFORMING ORGANIZATION NAME AND ADDRESS
Grumman Aerospace Corporation
Bethpage, N. Y. 11714

10. WORK UNIT NO.

11. CONTRACT OR GRANT NO.: NAS 8-28728

12. SPONSORING AGENCY NAME AND ADDRESS
National Aeronautics and Space Administration
Washington D.C. 20546

13. TYPE OF REPORT & PERIOD COVERED: Contractor Report

14. SPONSORING AGENCY CODE

15. SUPPLEMENTARY NOTES

16. ABSTRACT

Six nickel - 12 wt percent tin samples were processed in the M-553 Sphere Forming Experiment on Skylab II. These samples were distributed and evaluated as follows:

1.6	University of Connecticut
1.3	Georgia Tech
1.4 & 2.7	Arthur D. Little, Inc.
1.5 and 2.3	Grumman Aerospace Corporation

These results are presented and compared with the results generated during ground based (1-g) and KC-135 (low-gravity) simulation. The samples have been characterized with respect to sphericity, density, porosity, surface morphology, segregation, contamination, microhardness, chemical composition, Curie point, and crystallographic features. These results will be discussed with regard to the simulation studies and the literature; conclusions will be drawn and recommendations made.

17. KEY WORDS	18. DISTRIBUTION STATEMENT
	Unclassified - Unlimited

19. SECURITY CLASSIF. (of this report)	20. SECURITY CLASSIF. (of this page)	21. NO. OF PAGES	22. PRICE
Unclassified	Unclassified	18	NTIS

NICKEL - 12 WT % TIN ALLOY EVALUATION

SUMMARY

Six nickel - 12 wt % tin samples were processed in the M-553 Sphere Forming Experiment on Skylab II. These samples were distributed and evaluated as follows:

1.6	University of Connecticut
1.3	Georgia Tech
1.4 and 2.7	Arthur D. Little, Inc.
1.5 and 2.3	Grumman Aerospace Corporation

These results are presented and compared with the results generated during ground based (1-g) and KC-135 (low-gravity) simulation. The samples have been characterized with respect to sphericity, density, porosity, surface morphology, segregation, contamination, microhardness, chemical composition, Curie point, and crystallographic features. These results will be discussed with regard to the simulation studies and the literature; conclusions will be drawn and recommendations made.

CHARACTERIZATION RESULTS AND DISCUSSION

Sphericity. It cannot be said that in every case the degree of sphericity of the flight specimens was superior; however, it may safely be stated that the best examples of spherical specimens in zero gravity were superior to those in one gravity.

Two techniques were utilized to monitor sphericity. The first technique used was a micrometric examination that determined the maximum and minimum diameters of the specimens and the ratio of these numbers is included in Table 1 as degree of sphericity. Alternatively, a shadowgraph was utilized to determine the sphere radii in three orthogonal directions. Figure 1 illustrates the latter technique. Results from the two techniques were comparable.

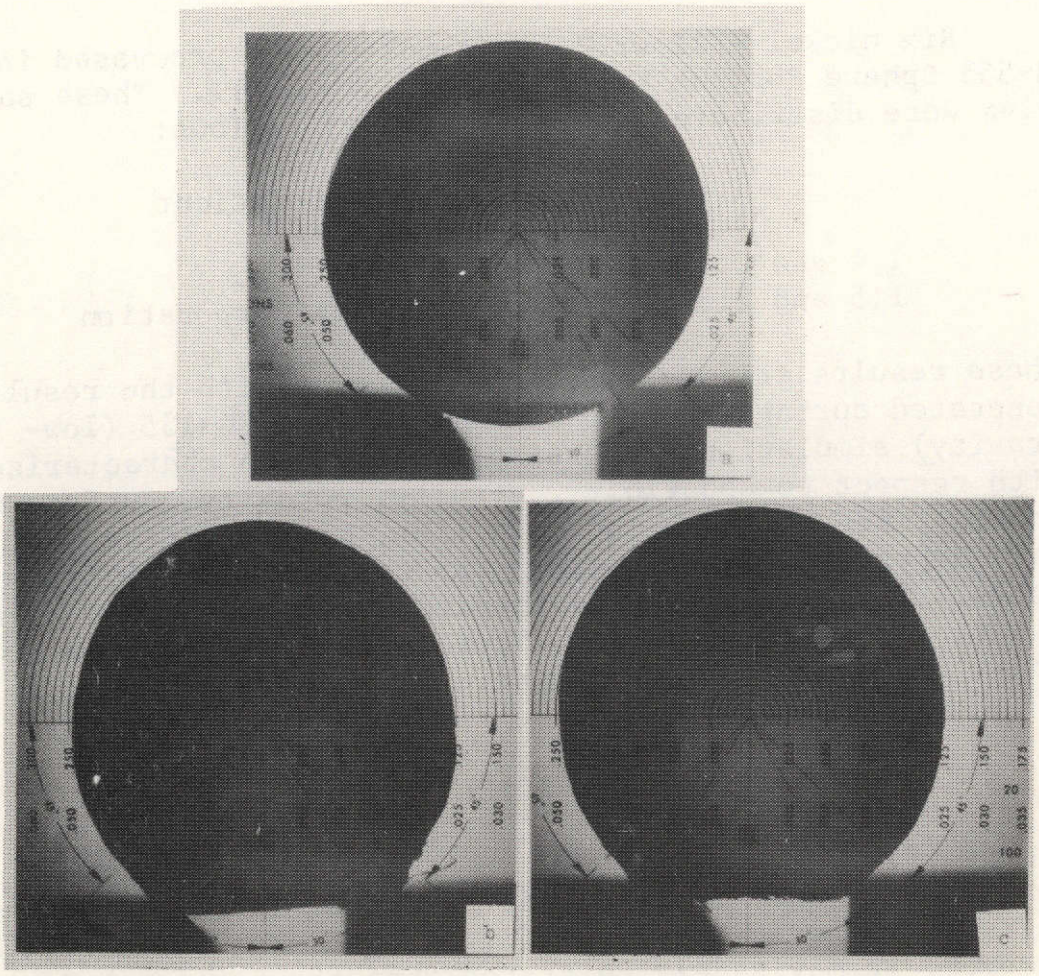

Figure 1. Shadowgraphs of Specimen 1.6. (a) Top View, (b) and (c) Orthogonal Side Views (10X).

Also included in this and in subsequent tables are data generated from the ground base sample 1-7.

TABLE 1. TABULATION OF WEIGHT (GM), DENSITY (GM/cc), AND DEGREE OF SPHERICITY

Sample Number	Degree of Sphericity	Weight (GM)	Density (GM/cc)
1-3	N.A.	1.21442	9.29
1-4	1.285	1.24746	9.09
1-5	1.04	1.21621	8.87
1-6	1.06	1.21465	9.01, 7.85
2-3	1.015	1.27565	9.25
2-7	1.023	1.21125	9.19
G1-7	1.16	N.A.	8.07

N.A. - Not Available

Density and Porosity. The density and weights of the samples are tabulated in Table 1. No great variation in weight is noted, and the slightly greater weight associated with samples 1-4 and 2-3 is due to portions of the sting being retained. The densities are those supplied by MSFC with the samples. However, in the one case where the density value was carefully checked, there was found to be substantial disagreement. The latter value is preferred as it is more consistent with the level of porosity monitored quantitatively by microscopic examination. The discrepancy may be attributed to unfavorable sample configuration that makes this type of measurement difficult.

Figure 2 shows a macrophotograph of a transverse section of sample 2-7. It is clear that there is substantial interdendritic void area caused by solidification shrinkage, as well as a large circular pore. This porosity, since it is connected to the sample surface, makes a density measurement difficult.

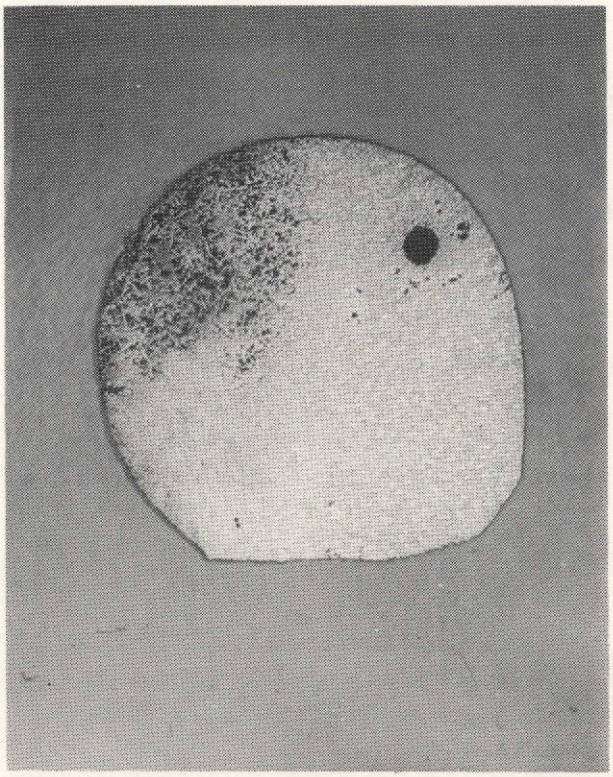

Figure 2. Macrophotograph of a Transverse Section of Sample 2-7 Showing Porosity (10X).

A calculation of the percent porosity, based on the lower density value for sample 1-6, gives a value of 10.08 percent, whereas quantitative metallography gave 9.17 percent. These may be compared with the ground base values of 8.40 and 7.40, respectively.

Individual pore sizes at the surface of sample 1-5 were typically 11 μm, whereas internal voids in sample 1-6 varied from 2 to 900 μm. The large pore in this sample, as in sample 2-7, should not be considered an interdendritic shrinkage cavity.

Surface Morphology. The surface morphology of the samples will be treated as a compilation rather than a reiterative analysis of individual samples.

Figure 3 is a macrophotograph of sample 1-5. The last region to solidify is marked by substantial shrinkage cavities. The cavities act as a line of demarkation between

the region of surface nucleation and growth (upper cap) and the epitaxial growth that has occurred from the region of the sting or the pedestal.

Surface nucleated growth appears two dimensional at low magnifications since no growth could occur radially outward from the liquid surface. Growth was, in fact, inward from these regions. These regions appear smooth and bright and are shown in the upper portion of Figure 4.

Epitaxial growth occurs from the sting, pedestal, or remnant unmelted solid areas and progresses from these regions. These dendrites penetrate into the liquid and if they are at the surface and in a last region to solidify, then the last liquid is drawn from around them. This results in their appearing three dimensional, not flat and dull. These are shown in the lower portion of Figure 4. Enlargements of surface nucleated dendrites (two dimensional) and free dendrites (three dimensional) are shown in Figures 5 and 6, respectively.

Sample 2-3 exhibited no distinct interfacial region between the surface nucleated and free dendrites. In fact, the sample appearance indicated that virtually the entire sample was surface nucleated and grown. This morphology is shown in Figure 7. Flat islands and dimpled regions should be noted, and enlargements of these features are shown in Figures 8 and 9, respectively. These show differing types of growth terraces and whereas Figure 8 clearly identifies the flat islands as being associated with platelet growth, it is not entirely certain whether the dimpled regions are representative of an unusual cellular or cellular dendritic growth. Other regions of sample 2-3 were similar to Figure 5.

An interesting feature noted on sample 2-3 was that a microchemical mapping of tin content across one of the flat islands and a similar mapping of a sectioned secondary dendrite arm gave exactly the same results with respect to solute content versus distance grown. This is an intriguing result in that it shows that the solute content was not as critical in deciding the solidification morphology as were the thermal parameters (G and R).

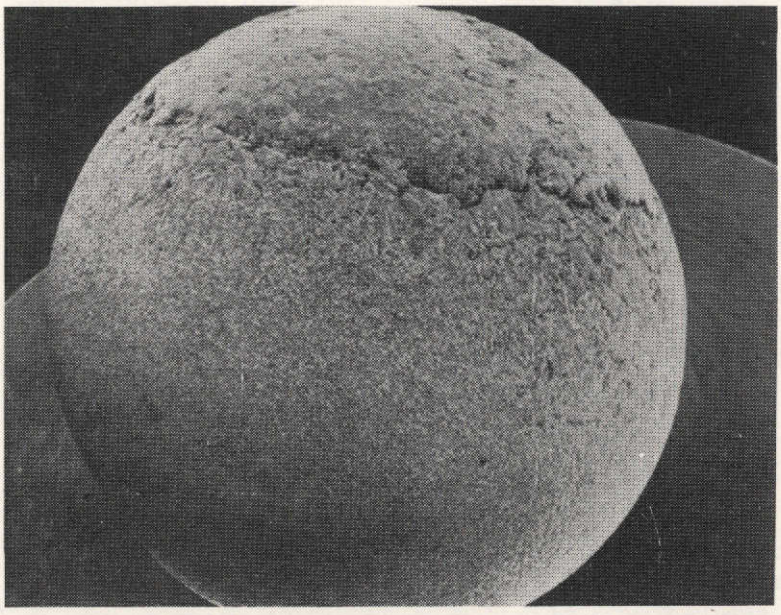

Figure 3. Macrophotograph of Sample 1-5 Showing Regions of Surface Nucleated and Free Dendrites (~ 10X).

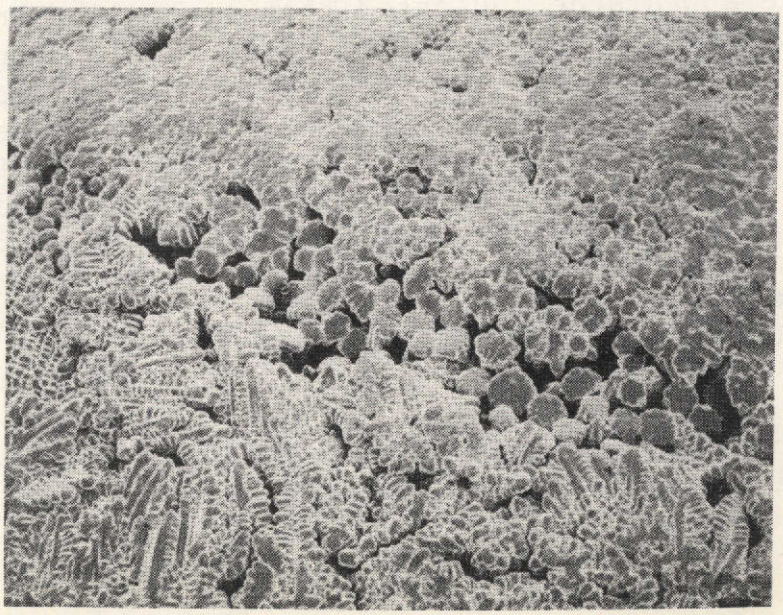

Figure 4. Interface Between Surface Nucleated and Free Dendrites (100X). Sample 1-5.

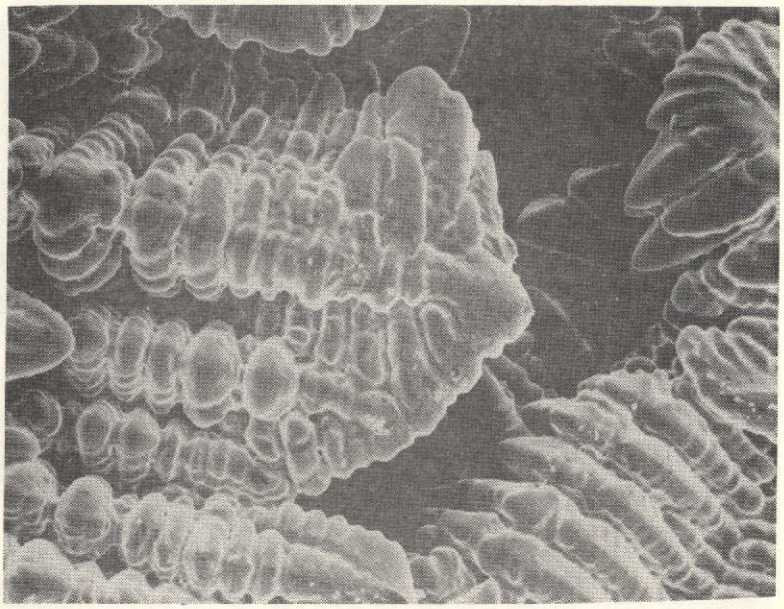

Figure 5. Micrograph of Free Dendrites in a Region of Interdendritic Shrinkage Cavities (1500X).

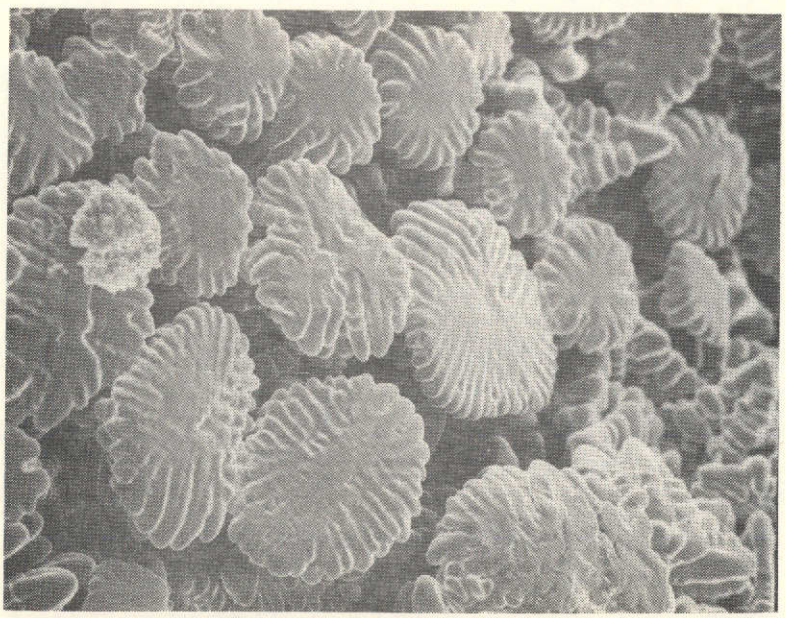

Figure 6. Micrograph Showing Surface Nucleated Dendrites in a Region of Interdendritic Shrinkage Cavities (200X).

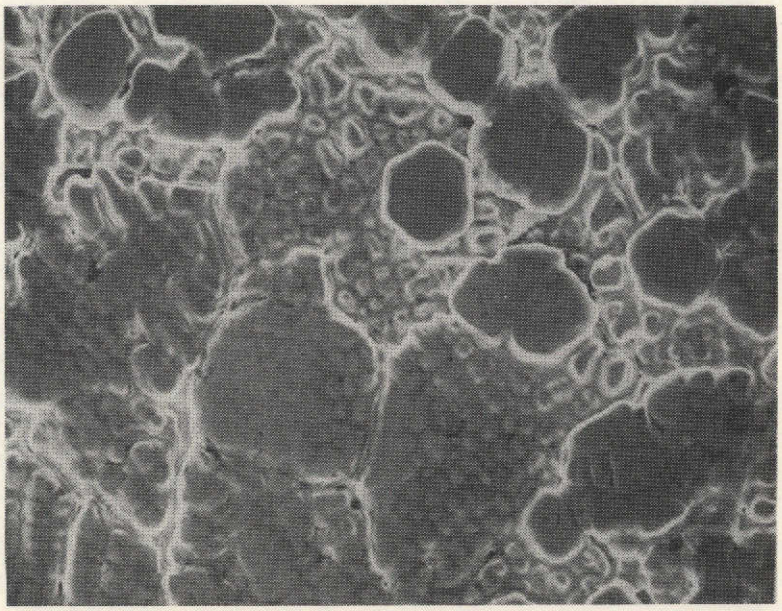

Figure 7. Micrograph Showing Platelet and Dimpled Morphologies in Surface Nucleated Regions of Sample 2-3 (400X).

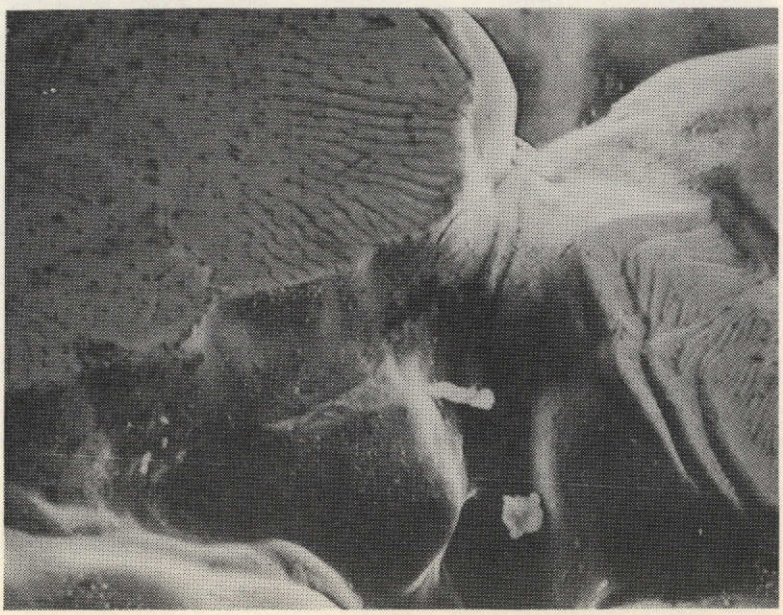

Figure 8. Micrograph Showing Growth Terraces During Platelet Solidification in Surface Nucleated Regions of Sample 2-3 (3750X).

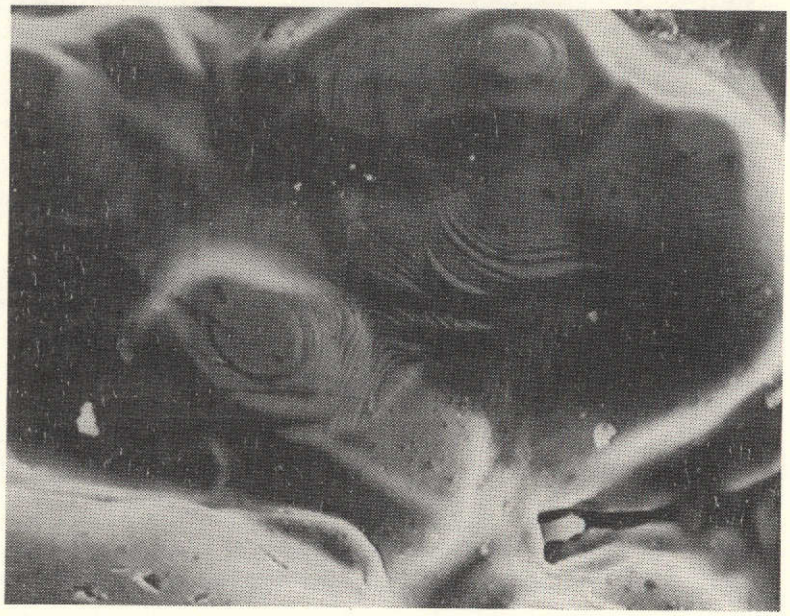

Figure 9. Micrograph Showing Growth Terraces in Surface Nucleated, Dimpled, Regions of Sample 2-3 (3750X).

At this point it is perhaps appropriate to consider the solidification mechanism more carefully. There are two aspects that should be considered, the liquid→solid attachment mechanism and the distribution of solute in the liquid ahead of the advancing solid front. If we look at the last regions to solidify, we may find a "record" of the last stages of this process. Figure 10 illustrates that we have an outstanding record of both of these processes. With regard to the growth mechanism, growth spirals close to a {111} orientation are clearly evident. What is also significant, however, is that the solute has been redistributed in a highly localized fashion and is lying principally on {100}<110> systems. The highly localized nature of this redistribution was unanticipated. Figure 11 shows a differing spiral or ring mechanism with different solute redistribution and Figure 12 shows yet another array. These arrays and mechanisms should be fully documented, analyzed crystallographically, and mapped compositionally.

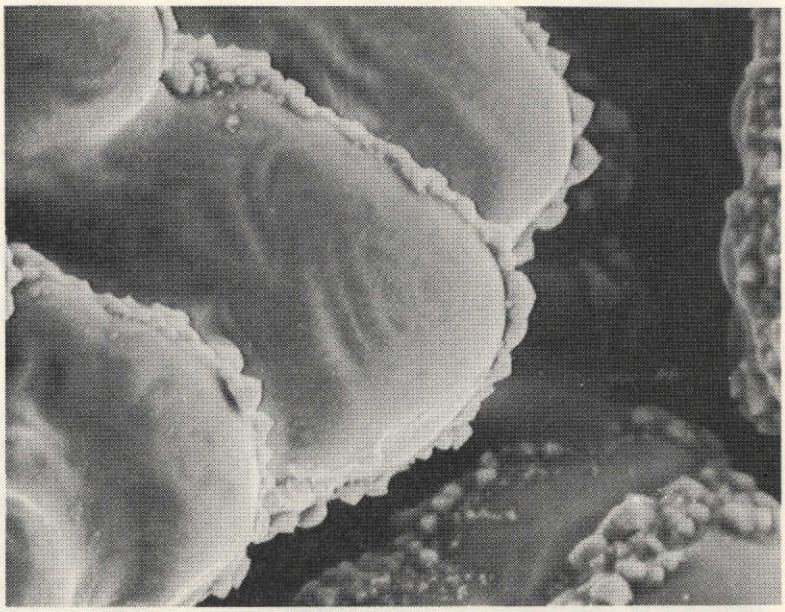

Figure 10. Micrograph Showing Dendritic Growth Spiral and Highly Localized Lateral Solute Segregation to {100}<110> Regions of the Dendrite (3750X).

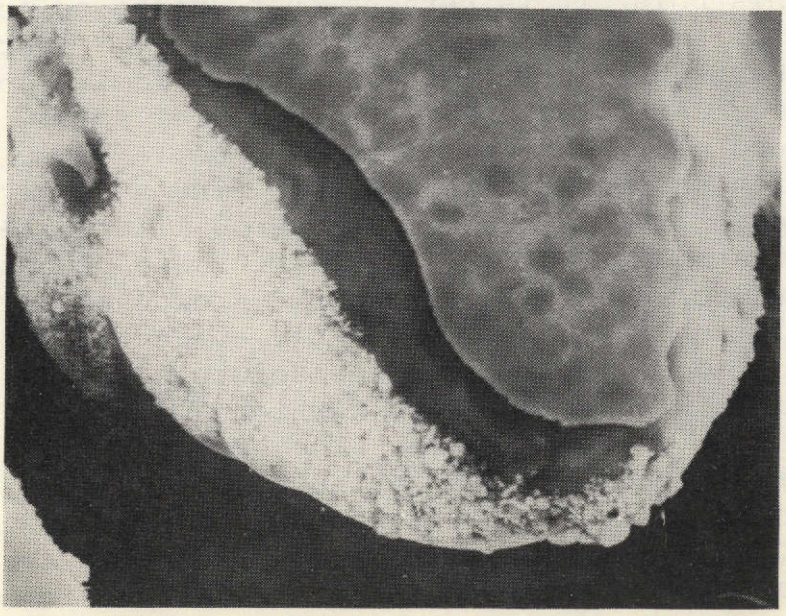

Figure 11. Micrograph Showing Dendritic Growth Terrace and Different Array of Solute (3750X). Sample 2-3.

Internal Grain Morphology. The interior microstructures noted were of four distinct types: remnant unmelted solid, epitaxial dendrites growing from the prior region, free dendrites, and an irregular dendritic array that would appear to be almost a divorced eutectic. Figure 13 shows remnant unmelted solid, epitaxial dendrites and free dendrites, whereas Figure 14 shows the irregular dendritic pattern and Figure 15 (at higher magnification) shows the divorced nature of the reaction.

The epitaxial dendrites were typically 1000 ± 200 μm long and 100 ± 50 μm wide. The coarse free dendrites (equiaxed) were typically 200 μm and the fine irregular microstructure showed a grain size of approximately 100 μm. The latter structure does not seem to have been documented during the ground base studies.

The columnar dendrites typically had a secondary dendrite arm spacing of 15 μm and this increased with distance from the ceramic substrate or unmelted solid. In the region of free, coarse, dendrites, 22 μm was typical. Nonequilibrium second phase was located in the interdendritic regions and the average volume fraction was 0.069 ± 0.005. In the irregular microstructure, the volume fraction of second phase was 0.063 ± 0.008.

One last internal feature should be noted, and that is the large spherical pore shown in Figures 2 and 14. This type of pore was found in samples 1-6 and 2-7. In the former it was 900 μm and in the latter it was 200 μm. These had not been noted in ground base prepared specimens. This was likely to have been formed because the partial pressure of the constituent elements at these elevated temperatures and low chamber vacuums, was no longer negligible. Consideration of a pressure/temperature projection for the Ni-Sn system, and in the pressure range of interest, leads to the immediate conclusion that the phase diagram does not apply, nor does an assumption of anything approaching equilibria. Further consideration of reduced pressure phase reactions that can occur points to the fact that $L \Rightarrow G \Rightarrow L$ reactions are plausible and if this were a portion of the reaction sequence then a spherical cavity would be formed. Terrestially, the vast density differences

Figure 12. Micrograph Showing Decorated Growth Terraces of Sample 1-6 (1000X).

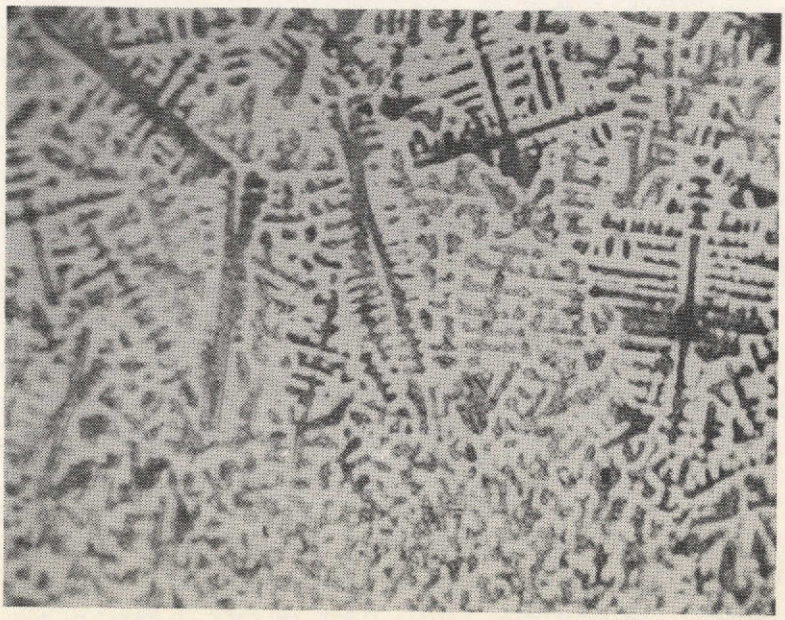

Figure 13. Optical Micrograph Showing Remnant Unmelted Solid, Epitaxial Dendrites, and Free (Equiaxed) Dendrites (100X). Sample 2-3.

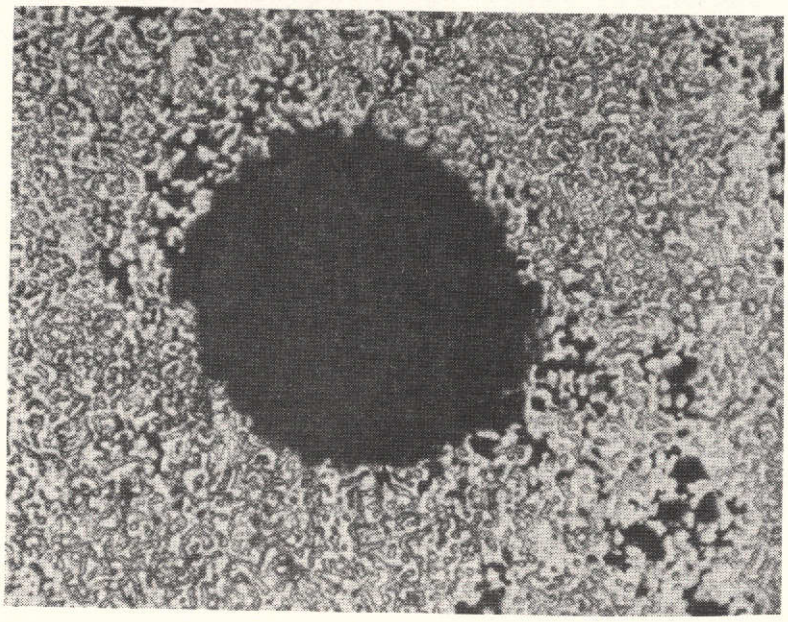

Figure 14. Optical Micrograph Showing Irregular Solidification Morphology and Large Spherical Pore in Sample 2-7 (100X).

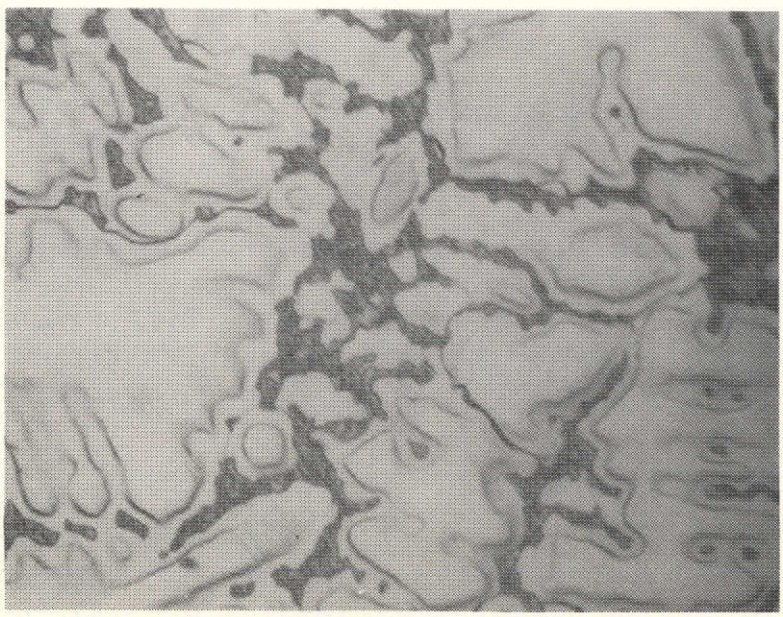

Figure 15. Optical Micrograph Showing the Above Structure at a Higher Magnification (500X).

between liquid and vapor would result in the vapor being emitted. However, in zero gravity there is no such density difference and the vapor is trapped.

Segregation. The minimum tin concentration found in the platelet, epitaxial dendrite, or free dendrite growths was 4.25 wt percent in each case. The maximum reported was 15.56 wt percent. Interdendritic compositions varied from a low of 22.86 wt percent to a high of 32.42 wt percent. The highest local segregation ratio monitored was 9.91 on sample 2-3 and the lowest was 2.69 on sample 1-5.

Contamination. The samples reflected, in surface analysis, that they were contaminated both by the vapor deposition from adjacent samples, and from the pedestal material (Al_2O_3). Table 2 shows typical surface analyses for samples 1-5 and 2-3.

Microhardness. The microhardness of the samples was reasonably consistent and was such that the primary dendrites were approximately 260 ± 10 VHN, the intermetallic was 500 ± 20 VHN, and the dendrite arm boundaries were 280 ± 5 VHN. This is entirely consistent with the ground base samples.

Chemical Compositions. Bulk analyses of tin concentration were conducted on sample 1-6. It was found to contain 10.05 wt percent Sn.

Analysis of gases was: O/20 PPM, N/4 PPM, H/2 PPM. Analysis of other elements was: Si/5 PPM, Mg/5 PPM, Cr/5 PPM, Cu/15 PPM, Zn + Pb/10 PPM, Ti/5 PPM, Co/5 PPM, Fe/10 PPM, C/10 PPM. Analytical results from ground base sample 1-7 was 10.30 wt percent Sn and substantially the same for everything else.

Curie Point. The Curie points monitored for samples 1-5 and 2-3 were 189°C and 175°C, respectively. This is substantially higher than the 108°C. Curie point measured for the as received material. This is probably an indication that there has been appreciable tin loss during processing. Since tin has a substantially higher vapor pressure than nickel does at these temperatures, this is to be expected.

TABLE 2. ELEMENTAL ANALYSIS OF SURFACE REGIONS

Sample Number	Region	Nominal Comp. (Wt %)	Al	W	Ag	Sn	Ni	Cu	Fe	Cr
1.5	Side (Avg. of Three Orthogonal Directions)	Ni-12 Sn	1.01	0	0.33	5.50	91.72	1.13	0	0.31
	Top	Ni-12 Sn	1.04	0.44	0.03	6.74	91.07	0.73	0.12	0
2.3	Side (Avg. of Three Orthogonal Directions)	Ni-12 Sn	21.40	0	19.5	0.88	56.18	1.25	0.44	0.39
	Top	Ni-12 Sn	2.81	0	1.25	2.09	92.43	1.20	0.21	0

Note: Technique - EDAX

Crystal Structure. The dendritic solidification results in tin rich and tin depleted regions of the sample. This is reflected in the lattice parameter of the face centered cubic material. Sample 2-3 had a solute rich parameter of 3.6000Å. Sample 1-5 has a solute rich lattice parameter of 3.5993Å and a solute poor composition of 3.5701Å. These are mean bulk parameters of 3.5783 and 3.5779, respectively.

Our ground base results for samples 2-3 and 2-12 gave solute rich lattice parameters of 3.608 and 3.611Å, respectively, and solute poor values of 3.549 and 3.552, respectively, and median bulk values of 3.578 and 3.582.

These data would indicate that sample 2-3 is substantially the same as the ground base samples, but sample 1-5 shows less lattice parameter spread.

CONCLUSIONS

The results and discussion sections have shown that the primary beneficial findings are on a microscopic and microchemical scale, and are not obvious features.

We have demonstrated that an outstanding record exists of growth mechanisms and solute redistribution within these samples. This preliminary work should be pursued in order to maximize the fundamental knowledge derived from these samples. Detailed analysis of these structures and testing of these results against existent solidification theory should allow a much better picture of the solidification process to be drawn.

We have also shown that the partial pressures of constituent elements can play a significant role in processing of this type. This work should be pursued as it advances space processing from strictly liquid/solid processing to liquid/solid/gas processing. This opens up an enormous number of new processing reactions and, as a result, new structures and morphologies.

Lastly, we have in the specimens an outstanding record of solute redistribution processes. This record, too, should be carefully pursued, mapped, and tested against existent solute redistribution theory.

☆ U.S. GOVERNMENT PRINTING OFFICE 1974 – 640-446 / 110 REGION NO. 4